A Kirkwood−Buff Derived Force Field for Methanol and Aqueous Methanol Solutions

Samantha Weerasinghe and Paul E. Smith*

Department of Chemistry, University of Ruhuna, Matara, Sri Lanka, and Department of Chemistry, Kansas State University, Manhattan, Kansas 66506-3701

Received: April 6, 2005; In Final Form: June 6, 2005

A force field for the simulation of methanol and aqueous methanol mixtures is presented. The force field was specifically designed to reproduce the experimental Kirkwood−Buff integrals as a function of methanol mole fraction, thereby ensuring a reasonable description of the methanol cosolvent and water solvent activities. Other thermodynamic and physical properties of pure methanol and aqueous methanol solutions, including the density, enthalpy of mixing, translational diffusion constants, compressibility, thermal expansion, and dielectric properties, were also well reproduced.

Introduction

The accuracy of results obtained from simulation studies can only be as good as the quality of the force field describing the intermolecular and intramolecular interactions. Consequently, there is a constant need for improved force fields which better reproduce the available experimental data for a wide range of systems. Recently, we have been developing a series of force fields which were specifically designed to reproduce the experimental Kirkwood−Buff (KB) integrals for condensed phase solution mixtures.[1−4] These KB derived force fields (KBFF) have been shown to reasonably reproduce not only the KB integrals, but also other thermodynamic and physical properties of aqueous solution mixtures. The main advantages of this type of approach are the increased data for parametrization, especially useful for salts,[3,4] and an ability to easily determine the activity (chemical potential) of the cosolvent and water as a function of composition. The latter being very sensitive to the force field parameters being used.[5]

The KBFF approach is primarily aimed at providing accurate force fields for the simulation studies of cosolvent effects on peptides and proteins as a knowledge of the cosolvent activity is required.[6,7] In this study we extend our approach to the study of methanol and aqueous methanol solutions as a model for both alcohols and the serine and threonine amino acid side chains. Several force fields for methanol have been proposed,[8−22] and a range of simulations of methanol and aqueous methanol solutions have been performed.[23−35] However, to our knowledge, none have attempted to reproduce the experimental KB integrals. Unfortunately, our previous work has also shown that many existing force fields perform poorly in their ability to reproduce these integrals.[1−3,5,36,37] The present force field represents a simple united atom nonpolarizable force field that can be used with most biomolecular simulation packages. The force field is designed for use with the SPC/E water model,[38] but tests with other simple three-site models suggest the differences are usually negligible.[1−4]

Methods

Kirkwood−Buff Analysis of the Experimental Data. An analysis of the experimental data for methanol cosolvent (c) and water (w) mixtures was performed as outlined by Ben-Naim.[39,40] The Kirkwood−Buff integrals (G_{ij}) are defined as,[41]

$$G_{ij} = 4\pi\int_0^\infty [g_{ij}^{\mu VT}(r) - 1]r^2\,\mathrm{d}r \tag{1}$$

where g_{ij} is the corresponding radial distribution function (rdf). The above integrals measure the deviation of intermolecular distribution from random. The KB integrals can be obtained from experimental data on the chemical potentials (μ_i), partial molar volumes ($\bar{V}_i$), and isothermal compressibilities (κ_T) of the binary mixtures at constant pressure (p) and temperature (T) according to,[42]

$$G_{ij} = RT\kappa_T - \frac{\bar{V}_i\bar{V}_j}{(1 + f_{cc})V_m}$$

and

$$G_{ii} = G_{ij} + \frac{1}{x_i}\left(\frac{\bar{V}_j}{1 + f_{cc}} - V_m\right) \tag{2}$$

where R is the gas constant, x_i is the mole fraction of i, $V_m = V/(N_c + N_w)$ is the molar volume, and

$$\beta\left(\frac{\partial\mu_c}{\partial \ln x_c}\right)_{p,T} = 1 + \left(\frac{\partial \ln f_c}{\partial \ln x_c}\right)_{p,T} = 1 + f_{cc} \tag{3}$$

with ($\beta = 1/RT$) and f_c equal to the cosolvent activity coefficient on the mole fraction scale with the pure cosolvent solution as the standard state.

Partial molar volumes were determined from the experimental density data[43] by calculating the excess molar volume,

$$X_m^E = X_m - x_c X_{m,c}^0 - x_w X_{m,w}^0 \tag{4}$$

where X is the volume (V) of the solution and $V_{m,i}^0$ is the molar volume of pure i. The raw data were then fitted to a Redlich−Kister equation,[44]

$$X_m^E = x_c x_w \sum_{i=0}^{n} a_i (x_w - x_c)^i \tag{5}$$

where a_i are fitting constants. The partial molar volumes at any composition are then given by,

* Address correspondence to this author at Kansas State University. Phone: 785-532-5109. Fax: 785-532-6666. E-mail:pesmith@ksu.edu.

10.1021/jp051773i CCC: $30.25
Published on Web 07/19/2005

$$Y_i = X_m^E - x_j\left(\frac{\partial X_m^E}{\partial x_j}\right)_{p,T} \quad (6)$$

with $Y = \bar{V}_m^E$ and $X = V$. In general, the KB integrals are not sensitive to the exact values of the isothermal compressibility and therefore the following approximate expression was used,[42]

$$\kappa_T = \phi_c\kappa_{T,c}^0 + \phi_w\kappa_{T,w}^0 \quad (7)$$

where $\varphi_i = \rho_i\bar{V}_i$ is the volume fraction of i in the solution. Isothermal compressibilities for the pure solutions ($\kappa_{T,i}^0$) were taken from the literature.[45]

The excess molar Gibbs energy (G_m^E) was obtained by assuming the form given in eq 5 with $X = \beta G$, and then fitting the excess chemical potentials ($\beta\mu_i^E = \ln f_i$) of both methanol and water to the experimental data[46] using eq 6 with $Y_i = \ln f_i$ and $X = \beta G$. The resulting data are in agreement with previous determinations of the excess and partial molar volumes of methanol and water,[45,47,48] and a previous determination of the KB integrals for regions where the KB integrals are statistically reliable.[42]

Molecular Dynamics Simulations. All mixtures were simulated using classical molecular dynamics techniques and the SPC/E water model.[38] The simulations were performed in the isothermal isobaric (NpT) ensemble at 300 K and 1 atm. The weak coupling technique[49] was used to modulate the temperature and pressure with relaxation times of 0.1 and 0.5 ps, respectively. All bonds were constrained using SHAKE[50] and a relative tolerance of 10^{-4}, allowing a 2 fs time step for integration of the equations of motion. The particle mesh Ewald technique was used to evaluate the electrostatic interactions.[51] A real space convergence parameter of 3.5 nm^{-1} was used in combination with twin range cutoffs of 0.8 and 1.5 nm, and a nonbonded update frequency of 10 steps. The reciprocal space sum was evaluated on a 60^3 grid with $\leq$0.1 nm resolution. Random initial configurations of 2000 molecules in a cubic box were used. The steepest descent method was then used to perform 100 steps of minimization. This was followed by extensive equilibration, which was continued until all intermolecular potential energy contributions and rdfs displayed no drift with time (typically 1 ns). Configurations were saved every 0.1 ps for analysis.

Translational self-diffusion constants (D_i) were determined using the mean square fluctuation approach,[52] relative permittivities (ϵ) and the Debye relaxation time (τ_D) from the dipole moment fluctuations and correlation function,[53] the finite difference compressibilities (κ_T) by performing additional simulations of 250 ps at 250 atm,[11] the finite difference heat capacity (C_P) and thermal expansion coefficients (α) from additional simulations of 250 ps simulations at 320 K,[11] shear viscosity (η) from the off-diagonal elements of the pressure tensor,[54] and excess enthalpies of mixing (ΔH_m^E) and heat of vaporization (ΔH_{vap}) from the average potential energies (E_{pot}).[11] Errors ($\pm 1\sigma$) in the simulation data were estimated by using two or three block averages.

Parameter Development. The force field used in this study involves a Lennard-Jones (LJ) 6-12 plus Coulomb potential, together with the SPC/E water model. Our previous studies used a simple scheme to obtain polar atom parameters for the LJ term,[1] and the same approach is used here. United atom methyl group parameters were taken from the literature.[55] The molecular geometry was taken from the OPLS force field.[22] The charges on the atoms were then adjusted (two-parameter fit) to best reproduce the density and KB integrals for solution mixtures with $x_c = 0.25$, 0.50, and 0.75. Approximately 20 trial charge distributions were studied with values of q_O ranging between -0.70 and -0.90, and values of q_H ranging between 0.40 and 0.60. Partial atomic charges outside these ranges did not result in reasonable values of the KB integrals. The final parameters are presented in Table 1. The molecular dipole moment of 2.59 D lies between the gas-phase value of 1.7 D[56] and the estimated liquid-phase value of 2.9 D,[57] as is observed for the SPC/E water model.[38] It is similar to the average values observed for a recent fluctuating charge model for methanol (2.42 D),[12] to a density functional simulation (2.59 D),[28] a Car-Parrinello simulation (2.64 D),[30] and an induced dipole model (2.42 D),[10] but lower than the induced dipole model of Dang and Chang (2.8 D).[13]

TABLE 1: Nonbonded Force Field Parameters Used in the Simulations[a]

model	atom	ϵ, kJ/mol	σ, nm	q, |e|
methanol				
KBFF	O	0.6506	0.3192	−0.82
	H	0.0880	0.1580	0.52
	CH_3	0.8672	0.3748	0.30
water				
SPC/E	O	0.6506	0.3166	−0.8476
	H			0.4238

[a] Parameters for the SPC/E water model were taken from ref 38. The methanol geometry of O−H = 0.0945 nm, CH_3−O = 0.143 nm, and angle 108.5° (CH_3−H = 0.1948 nm) was taken from ref 22. All intramolecular bond distances were constrained using SHAKE. The dipole moment for the KBFF model is 2.59 D. Geometric mean combination rules were applied for both the ϵ_{ij} and σ_{ij} parameters.

Kirkwood−Buff Analysis of the Simulated Data. The KB integrals obtained from an analysis of the experimental data correspond to integrals over rdfs in the μVT ensemble. The simulated KB integrals were obtained by assuming that,[1,4,7]

$$G_{ij} = 4\pi\int_0^\infty [g_{ij}^{\mu VT}(r) - 1]r^2\,dr \approx 4\pi\int_0^R [g_{ij}^{NpT}(r) - 1]r^2\,dr \quad (8)$$

where R is a cutoff distance at which the rdfs are essentially unity, i.e., the bulk solution values. In practice, this condition is difficult to achieve precisely unless one uses very large systems. However, a reasonable approximation is to determine $G_{ij}(R)$ and average the values over a short distance range, typically one molecular diameter.[1,4] In this work the final KB integral values have been obtained by averaging between 0.95 and 1.20 nm. Further justification for this approximation can be found in the Results section.

Using the simulated KB integrals one can determine the corresponding partial molar volumes,[40]

$$\bar{V}_i = \frac{1 + \rho_j(G_{jj} - G_{ij})}{\rho_i + \rho_j + \rho_i\rho_j\Delta G} \quad (9)$$

and activity derivative,

$$f_{cc} = \left(\frac{\partial \ln f_c}{\partial \ln x_c}\right)_{p,T} = -\frac{x_c\rho_w\Delta G}{1 + x_c\rho_w\Delta G} \quad (10)$$

where $\Delta G = G_{cc} + G_{ww} - 2G_{cw}$. The parameters used to describe the variation of the simulated G_m^E with composition (eq 5) were then obtained from the simulated values of f_{cc} and the thermodynamic relationship,

$$f_{cc} = x_c x_w \beta\left(\frac{\partial^2 G_m^E}{\partial x_c^2}\right)_{p,T} \quad (11)$$

TABLE 2: Summary of the Methanol and Water Simulations[a]

x_c	N_c	N_w	V, nm^3	ρ_c, M	ρ, g/cm^3	E_{pot}, kJ/mol	T_{sim}, ns
0.0	0	2000	60.16	0.0	0.995	−46.45	3
0.125	250	1750	68.47	6.1	0.959	−46.49	6
0.250	500	1500	77.22	10.8	0.925	−46.29	6
0.375	750	1250	86.43	14.4	0.894	−45.95	6
0.500	1000	1000	96.11	17.3	0.865	−45.51	6
0.625	1250	750	106.22	19.5	0.837	−45.00	6
0.750	1500	500	116.86	21.3	0.811	−44.37	6
0.875	1750	250	127.96	22.7	0.786	−43.58	6
1.0	2000	0	139.46	23.8	0.763	−42.60	3

[a] All simulations were performed at 300 K and 1 atm in the NpT ensemble. E_{pot} is the average potential energy per molecule and T_{sim} is the total simulation time. All other symbols have their usual meaning (see text). The molecular weight of methanol is 32.042 amu.

The isothermal compressibility was not determined from the KB integrals as it is typically statistically unreliable.

Results and Discussion

A summary of the simulations performed is presented in Table 2. They cover the entire composition range and all mixtures were simulated for 6 ns to ensure reasonable precision in the data. The oxygen-to-oxygen rdfs are displayed in Figure 1 as a function of composition. As would be expected for these two similar molecules, the rdfs displayed very similar positions for the maxima and minima. The first maximum increased and the first minimum decreased with methanol mole fraction. All rdfs were essentially unity beyond 1.0 nm. The most prominent feature was an increase in the first shell hydration for water to water suggesting an increasing degree of water self-association with increasing methanol mole fraction, in agreement with neutron diffraction data.[58] The corresponding first shell (R_m = 0.345 nm) coordination numbers are displayed in Figure 2. All three first shell coordination numbers displayed a linear dependence on methanol (or water) mole fraction, as observed previously.[29,35] The values in pure water were 5.1 compared to 2.0 in pure methanol. The experimental value for pure methanol is 1.9 at 0.34 nm.[59,60]

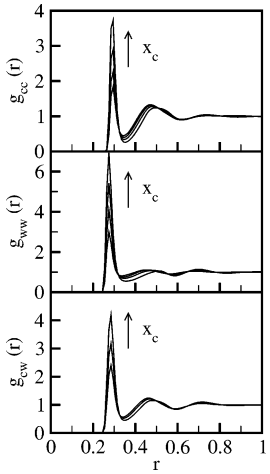

Figure 1. Oxygen to oxygen radial distribution functions as a function of distance (nm) and methanol mole fraction. Mole fractions of 0.0, 0.25, 0.50, 0.75, and 1.0 are displayed.

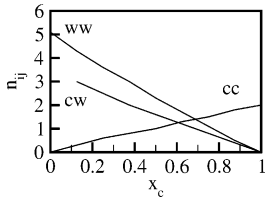

Figure 2. Oxygen to oxygen first shell (r < 0.345 nm) coordination numbers as a function of methanol mole fraction.

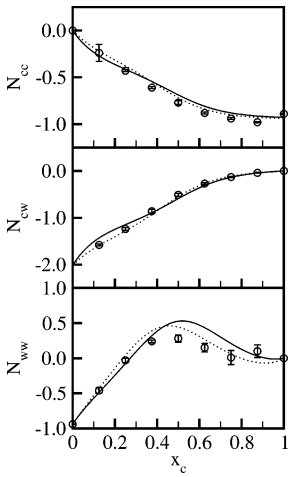

Figure 3. Excess coordination numbers ($N_{ij} = \rho_j G_{ij}$) as a function of methanol mole fraction. The solid lines correspond to the experimental data, the circles to the raw simulation data, and the dotted lines to the fitted simulation data.

TABLE 3: Fitting Constants for Equation 5

X		a_0	a_1	a_2	a_3	rmsd	units
βG	exp	0.5084	0.0653	−0.1678		0.01[a]	
	KBFF	0.4231	0.2494	−0.1613		0.01[b]	
βH	exp	−1.2842	−0.6012	−0.9008	−0.3699	0.001	
	KBFF	−1.5881	0.0796	−0.5017	−0.2279	0.001	
V	exp	−4.0382	−0.2727	0.5035	0.7093	0.006	cm^3/mol
	KBFF	−4.4378	0.1744	0.1691	−0.3215	0.004	cm^3/mol

[a] Obtained from a fit using eq 6. [b] Obtained from a fit using eq 11.

The experimental and simulated KB integrals are compared in Figure 3 as excess coordination numbers ($N_{ij} = \rho_j G_{ij}$). The use of excess coordination numbers helps to suppress the inherent uncertainties in both the experimental and simulated G_{ij} integrals at low j concentrations. The trends in the experimental data were well reproduced. There was essentially quantitative agreement for N_{cc} and N_{cw} over the whole composition range, whereas N_{ww} was underestimated slightly between x_c = 0.5 and 0.75. Also contained in Figure 3 are the excess coordination numbers obtained by performing a KB analysis but using the simulated densities and fits to βG_m^E as provided in Table 3. The fit suggests that the simulated KB integrals are in good agreement with experiment. Simulations of the x_c = 0.5 system performed with other three-site water models (SPC, TIP3P) produced little change in the simulated KB integrals (data not shown).

The experimental and simulated densities, partial molar volumes, and excess molar volumes are compared in Figure 4. The density of the pure methanol solution was slightly underestimated and hence one observes a gradually increasing deviation from the experimental density with increasing x_c. Analysis of the partial molar volumes suggested that this was due to a consistent overestimation in the methanol volume by 1 cm^3/mol. The water partial molar volume was quantitatively reproduced. By using the simulated density data one can obtain simulated partial molar volumes and excess molar volumes. If the truncation of the integral (eq 8) used in the KB analysis were unreasonable, then one would have expected some disagreement between the partial molar volumes obtained from

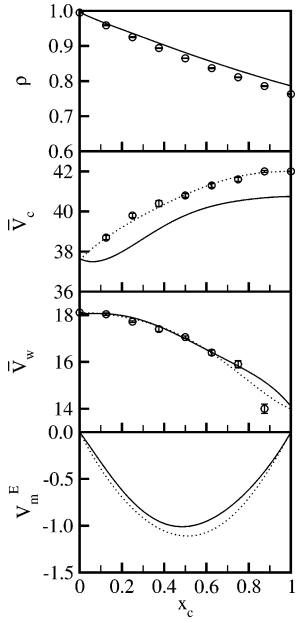

Figure 4. The density (g/cm^3), partial molar volumes, and excess molar volume (cm^3/mol) as a function of methanol mole fraction. The solid lines correspond to the experimental data,[43] the circles to the raw simulation data, and the dotted lines from a fit to the simulated density data.

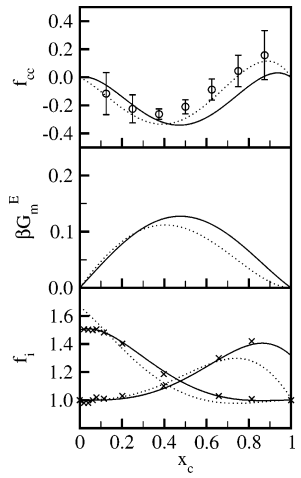

Figure 5. The activity derivative (f_{cc}), excess molar Gibbs energy (G_m^E), and mole fraction activity coefficients (f_i) as a function of methanol mole fraction. The solid lines and crosses correspond to the experimental data,[46] the circles to the raw simulation data, and the dotted lines to the fitted simulation data.

the simulated KB integrals and those obtained via the simulated densities. The data shown in Figure 4 suggested that this was not the case and implies the averaging of $G_{ij}(R)$ values between 0.95 and 1.20 nm captured the correct quantitative features of the integrals. The excess molar volume data indicated that, after correcting for the low simulated pure methanol density, the volume of the solution was actually slightly underestimated by the KBFF model. However, the differences of around 0.1 cm^3/mol were small.

Using eqs 10 and 11 and the simulated KB integrals one can obtain the required fitting constants for eq 5. The results are displayed in Table 3 and Figure 5. The oscillating behavior in f_{cc} was reproduced by the model and the variation of βG_m^E with composition was also well reproduced. Quantitative agreement was found for methanol mole fractions of <0.3, whereas βG_m^E was slightly underestimated for higher mole fractions. The

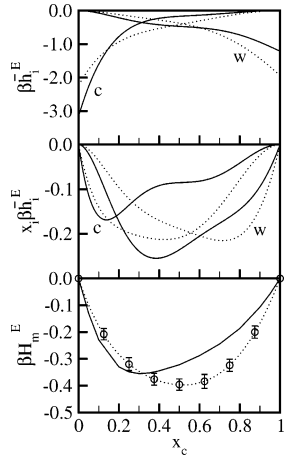

Figure 6. The excess partial molar enthalpies ($\bar{h}_i^E$), the contributions to the excess molar enthalpy ($x_i\bar{h}_i^E$), and excess molar enthalpy of mixing (H_m^E) as a function of methanol mole fraction. The solid lines correspond to the experimental data,[72] the circles to the raw simulation data, and the dotted lines to the fitted simulation data.

corresponding experimental and simulated activity coefficients are also displayed in Figure 5. The agreement for f_w was excellent except for very high methanol mole fractions. The agreement for f_c was less satisfactory but acceptable considering the sensitivity of the activity coefficients to the details of the force field.

The (excess) molar enthalpy of mixing is displayed in Figure 6. The simulated enthalpy was too favorable beyond $x_c = 0.3$. However, the differences are within those typically observed for other force fields.[11] By fitting the excess molar enthalpy to eq 5 with $Y = \beta H$, one obtains the parameters given in Table 3 which enable the separation of the excess molar enthalpy into partial molar enthalpies via eq 6 with $X = \beta H$ and $Y = \beta\bar{h}^E$. The results are also shown in Figure 6. The results indicate that both the water and methanol partial molar enthalpies were overestimated at some compositions and underestimated at others. This even occurred at low methanol mole fractions where the excess enthalpy of mixing was reasonably well reproduced. Hence, it is possible to obtain a good enthalpy of mixing from a particular model and yet the contributions from each component may be incorrect. In our opinion, there are two major possible sources for this discrepancy. Either composition-dependent polarization effects are significant, or the enthalpy contribution from composition-dependent vibrational and rotational frequency shifts have to be included for a more accurate comparison.[27,61] Both of these effects are absent from the current force field. However, the results are still reasonable.

The composition-dependent translational diffusion constants of both water and methanol are displayed in Figure 7. The experimental trends were well reproduced, although the exact compositions corresponding to the two minima were incorrect. This is to be expected as the diffusion constant for pure SPC/E water is higher than experiment, while the simulated value for methanol was lower than experiment. The isothermal compressibilities and relative permittivities of the solutions are displayed in Figure 8. Essentially quantitative agreement with experiment was observed with the compressibility of pure methanol only slightly underestimated.

The simulated properties of pure methanol are compared with experiment in Table 4. The most noticeable deviation occurred for the density, although the final value was reasonable in comparison with other force fields.[10,14,22] During the parametrization procedure it was observed that attempts to increase

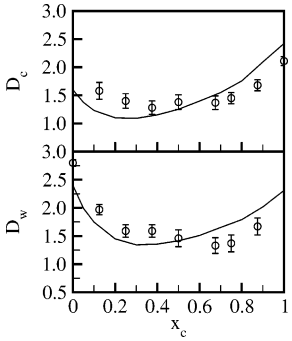

Figure 7. Methanol (D_c) and water (D_w) translational self-diffusion constants ($\times 10^{-9}$ m^2 s^{-1}) as a function of methanol mole fraction. The solid lines correspond to the experimental data,[73] and the circles to the simulation data. The experimental data have been scaled (<6%) using the pure solution values[56,69] to correct for isotopic substitution effects.

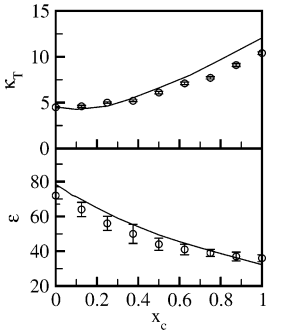

Figure 8. The isothermal compressibility (10^{-5} atm^{-1}) and relative permittivity as a function of methanol mole fraction. The solid lines correspond to the experimental data,[45,70] and the circles to the simulation data.

TABLE 4: Simulated and Experimental Properties of Pure Methanol at 300 K and 1 atm

property	KBFF[a]	exp	ref	units
ρ	0.763(1)	0.786	43	g/cm^3
E_{pot}	−42.60(2)			kJ/mol
ΔH_{vap}	37.6(1)	37.3	67	kJ/mol
D_c	2.1(1)	2.42	69	10^{-9} m^2/s
κ_T	10.4(2)	12.1	45	10^{-5} atm^{-1}
ϵ	36(3)	32.3	70	
τ_D	48(5)	49	64	ps
α	1.2(1)	1.2	45	10^{-3} K^{-1}
η	0.45(15)	0.54	71	cp
C_P	86(3)	80	68	J/mol/K
G_{cc}	−37.3(1)	−37.8	45	cm^3/mol

[a]Values in parentheses represent the estimated errors in the last decimal place.

the simulated density of pure methanol resulted in a very low diffusion constant, sometimes less than one-third of the experimental value. Hence, it was not possible to improve the density significantly without sacrificing agreement for other properties. The diffusion constant, compressibility, and thermal expansion coefficient for the KBFF model were all in good agreement with experiment. The shear viscosity value of 0.45 ± 0.15 cP was slightly low, although the differences between the various off-diagonal pressure tensor elements suggested there was considerable statistical uncertainty in the data when using just 1 ns of simulation.

The dielectric properties of pure methanol were well reproduced. The relative permittivity was determined from the dipole moment fluctuations as described previously,[62] using a reaction field perimittivity of $\epsilon_{RF} = \infty$ corresponding to the Ewald conducting boundary conditions. The final value of 36 ± 3 was

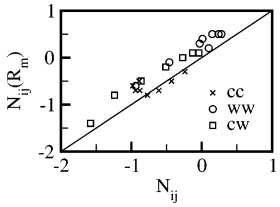

Figure 9. The correlation between simulated excess coordination numbers (N_{ij}) and the contribution from the first shell ($N_{ij}(R)$, $R = R_m = 0.345$ nm).

very close to the experimental value of 32.3. The total dipole moment correlation function decayed with a time constant of 48 ± 5 ps, equal to the Debye relaxation time (τ_D) for conducting boundary conditions,[63] again in excellent agreement with experiment. Finally, the infinite system Kirkwood g factor g_K was determined from the finite system g factor of $G_K = 3.6$ according to the boundary conditions.[62] The final value of $g_K = 2.5 \pm 0.2$ compared well with the experimental value of 2.9.[64] The overall agreement with experiment for the dielectric properties is an improvement over previous nonpolarizable models.[11,34]

The enthalpy of vaporization was determined from the average potential energy in the usual manner,[11] but included the polarization energy associated with condensed phase effective charges.[38] This was necessary to make the methanol model consistent with the SPC/E water model. Using the experimental gas-phase dipole moment of 1.7 D,[56] the molecular polarizability volume of 3.26×10^{-3} nm^3[3,47,65] together with the dipole moment of the KBFF model (2.59 D) resulted in a polarization energy of 7.3 kJ/mol. Also included in the vaporization enthalpy are the quantum corrections for the vibrational energies,[11,66] although these are small (−0.12 kJ/mol). The final value for the enthalpy of vaporization of 37.6 kJ/mol was in excellent agreement with the experimental value of 37.3 kJ/mol.[67]

The constant pressure heat capacity was determined from the variation in the system enthalpy with temperature using a finite difference approximation ($\Delta T = 20$ K).[11] A value of 80.5 J/mol/K for this derivative was determined from the simulations. The quantum corrections have been estimated previously as 5.7 J/mol/K,[11] and were included in the final value. The simulated value of 86 J/mol/K compares very favorably with the experimental value of 80 J/mol/K.[68]

The KB integrals quantify variations in the relative distribution of molecules over all solvation shells. It is interesting to compare these values with the corresponding values obtained on truncating the integral after the first solvation shell.[36] The excess first shell coordination numbers, $N_{ij}(R)$, obtained from eq 8 with $R = R_m = 0.345$ nm are compared to the full excess coordination numbers in Figure 9. A correlation exists between the first shell and full excess coordination numbers. However, with the exception of some N_{ww} values, the first shell numbers consistently underestimated the magnitude of the whole effect. This emphasizes that one needs to consider changes over several solvation shells to relate changes in solution structure to the thermodynamic properties of the solution.

The experimental and simulated oxygen-to-oxygen rdf for pure methanol is displayed in Figure 10. The agreement between the simulation and experiment was relatively poor, especially in comparison with other (polarizable) models.[12,13] The first peak was observed at a larger separation in the simulation (0.295 vs 0.267 nm), the same distance as that observed for pure SPC/E water, and probably explains the low density displayed by the model. Even so, the corresponding first shell coordination numbers were in good agreement (1.9 vs 2.0, see before).

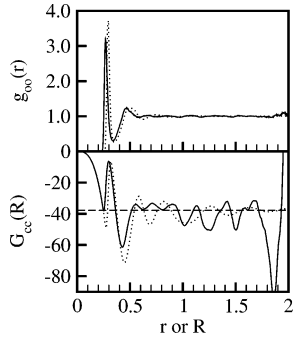

Figure 10. The oxygen-to-oxygen radial distribution function and corresponding KB integral (cm^3/mol) for pure methanol as a function of distance (r) or integration distance (R) in nm. The solid lines correspond to the experimental data,[59,60] while the dotted lines are from the simulated data. The dashed line corresponds to the KB integral obtained from the experimental isothermal compressibility.[40,45]

Comparison with the Patel and Brooks force field[12] suggested that the major difference in the parameter sets was the relatively large σ value for the hydroxyl hydrogen atom (0.158 vs 0.040 nm), which prevented a closer contact distance for hydrogen bonded oxygen pairs. Our van der Waals parameters were obtained from a simple scheme to reduce the degree of parametrization required for each system.[1] Hence, we decided not to modify the hydrogen parameters to improve the agreement with the experimental rdf in an effort to maintain a consistent force field approach. Furthermore, the good agreement with experiment observed for a variety of other properties suggested that this was not necessary.

Also shown in Figure 10 is the KB integral after integration of the rdf to a distance R. It was observed that the simulated value of G_{cc} (-37.3 cm^3/mol) was in agreement with the experimental value of -37.8 cm^3/mol,[45] even though the rdfs displayed significant differences. This raises an important issue when using the KB integrals for parametrization. If the same integral can be obtained from two different rdfs one cannot be certain that the final rdf, and therefore the set of partial atomic charges, is reasonable. However, in our experience,[1−4] the possibility of multiple solutions to the charge distribution has not been observed. In fact, it has often been difficult to find one set of atomic charges which reasonably reproduce the three KB integrals. This may be due to the fact that the van der Waals parameters were not allowed to vary during the parametrization procedure. It is quite possible that models with different densities can produce significantly different rdfs and yet very similar KB integrals. However, in our opinion, it will be unlikely that multiple parameter sets (for the same geometry) can simultaneously reproduce the experimental KB integrals and densities over a range of compositions.

Conclusions

A simple nonpolarizable three-site model for methanol has been determined by attempting to reproduce the experimental KB integrals for a series of aqueous methanol solutions. It was then shown that the model also reproduced a variety of other thermodynamic and physical properties which were not included in the original parametrization procedure. The model quantitatively reproduces the thermodynamic properties of mixtures of water and methanol up to methanol mole fractions of 0.3. At higher mole fractions small deviations are observed which appear to relate to deviations in the enthalpy of mixing and partial molar enthalpies of methanol and water. It is possible that these small deviations could be due to environmentally dependent polarization effects, although this is difficult to determine.

The final charge on the methanol oxygen was -0.82, which is significantly larger than that for many previous nonpolarizable force fields.[11,22] This is not too surprising as one can produce similar effective interactions between the hydroxyl groups by varying the charge and size (σ) parameters accordingly. Even so, it is satisfying that our alcohol and water oxygen parameters are very similar, as the electronegativities of carbon and hydrogen are very similar, and that this results in the correct balance between solvation of methanol by other methanol molecules and solvation by water molecules as displayed by the KB integrals.

Acknowledgment. This research was supported by the National Science Foundation. The authors thank Professor A. K. Soper for providing the experimental radial distribution function data for pure methanol.

References and Notes

(1) Weerasinghe, S.; Smith, P. E. *J. Phys. Chem. B* **2003**, *107*, 3891−3898.
(2) Weerasinghe, S.; Smith, P. E. *J. Chem. Phys.* **2003**, *118*, 10663−10670.
(3) Weerasinghe, S.; Smith, P. E. *J. Chem. Phys.* **2003**, *119*, 11342−11349.
(4) Weerasinghe, S.; Smith, P. E. *J. Chem. Phys.* **2004**, *121*, 2180−2186.
(5) Weerasinghe, S.; Smith, P. E. *J. Chem. Phys.* **2003**, *118*, 5901−5910.
(6) Timasheff, S. N. *Adv. Protein Chem.* **1998**, *51*, 355−433.
(7) Smith, P. E. *J. Phys. Chem. B* **2004**, *108*, 18716−18724.
(8) Stouten, P. F. W.; Kroon, J. *J. Mol. Struct.* **1988**, *177*, 467−475.
(9) Freitas, L. C. G. *THEOCHEM* **1993**, *101*, 151−158.
(10) Gao, J. L.; Habibollazadeh, D.; Shao, L. *J. Phys. Chem.* **1995**, *99*, 16460−16467.
(11) Walser, R.; Mark, A. E.; van Gunsteren, W. F.; Lauterbach, M.; Wipff, G. *J. Chem. Phys.* **2000**, *112*, 10450−10459.
(12) Patel, S.; Brooks, C. L. *J. Chem. Phys.* **2005**, *122*.
(13) Dang, L. X.; Chang, T. *J. Chem. Phys.* **2003**, *119*, 9851−9857.
(14) Caldwell, J. W.; Kollman, P. A. *J. Phys. Chem.* **1995**, *99*, 6208−6219.
(15) van Leeuwen, M. E.; Smit, B. *J. Phys. Chem.* **1995**, *99*, 1831−1833.
(16) Haughney, M.; Ferrario, M.; Mcdonald, I. R. *Mol. Phys.* **1986**, *58*, 849−853.
(17) Allinger, N. L.; Chen, K. H.; Lii, J. H.; Durkin, K. A. *J. Comput. Chem.* **2003**, *24*, 1447−1472.
(18) Jorgensen, W. L.; Maxwell, D. S.; Tirado-Rives, J. *J. Am. Chem. Soc.* **1996**, *118*, 11225−11236.
(19) Morrone, J. A.; Tuckerman, M. E. *Chem. Phys. Lett.* **2003**, *370*, 406−411.
(20) Chelli, R.; Pagliai, M.; Procacci, P.; Cardini, G.; Schettino, V. *J. Chem. Phys.* **2005**, *122*.
(21) Palinkas, G.; Hawlicka, E.; Heinzinger, K. *Chem. Phys.* **1991**, *158*, 65−76.
(22) Jorgensen, W. L. *J. Phys. Chem.* **1986**, *90*, 1276−1284.
(23) Stouten, P. F. W.; van Eijck, B. P.; Kroon, J. *J. Mol. Struct.* **1991**, *243*, 61−87.
(24) Haughney, M.; Ferrario, M.; Mcdonald, I. R. *J. Phys. Chem.* **1987**, *91*, 4934−4940.
(25) Palinkas, G.; Bako, I.; Heinzinger, K.; Bopp, P. *Mol. Phys.* **1991**, *73*, 897−915.
(26) Rivera, J. L.; McCabe, C.; Cummings, P. T. *Phys. Rev. E* **2003**, *67*, 011603.
(27) Venables, D. S.; Schmuttenmaer, C. A. *J. Chem. Phys.* **2000**, *113*, 11222−11236.
(28) Handgraaf, J. W.; Meijer, E. J.; Gaigeot, M. P. *J. Chem. Phys.* **2004**, *121*, 10111−10119.
(29) Laaksonen, A.; Kusalik, P. G.; Svishchev, I. M. *J. Phys. Chem. A* **1997**, *101*, 5910−5918.
(30) Pagliai, M.; Cardini, G.; Righini, R.; Schettino, V. *J. Chem. Phys.* **2003**, *119*, 6655−6662.
(31) Mountain, R. D. *Mol. Phys.* **1998**, *94*, 435−437.
(32) Richardi, J.; Millot, C.; Fries, P. H. *J. Chem. Phys.* **1999**, *110*, 1138−1147.
(33) Wheeler, D. R.; Rowley, R. L. *Mol. Phys.* **1998**, *94*, 555−564.
(34) Fonseca, T.; Ladanyi, B. M. *J. Chem. Phys.* **1990**, *93*, 8148−8155.
(35) Ferrario, M.; Haughney, M.; Mcdonald, I. R.; Klein, M. L. *J. Chem. Phys.* **1990**, *93*, 5156−5166.

(36) Chitra, R.; Smith, P. E. *J. Phys. Chem. B* **2001**, *105*, 11513−11522.
(37) Chitra, R.; Smith, P. E. *J. Chem. Phys.* **2001**, *115*, 5521−5530.
(38) Berendsen, H. J. C.; Grigera, J. R.; Straatsma, T. P. *J. Phys. Chem.* **1987**, *91*, 6269−6271.
(39) Ben-Naim, A. *J. Chem. Phys.* **1977**, *67*, 4884−4890.
(40) Ben-Naim, A. *Statistical Thermodynamics for Chemists and Biochemists*; Plenum Press: New York, 1992;
(41) Kirkwood, J. G.; Buff, F. P. *J. Chem. Phys.* **1951**, *19*, 774−777.
(42) Matteoli, E.; Lepori, L. *J. Chem. Phys.* **1984**, *80*, 2856−2863.
(43) Douheret, G.; Khadir, A.; Pal, A. *Thermochim. Acta* **1989**, *142*, 219−243.
(44) Redlich, O.; Kister, A. T. *Ind. Eng. Chem.* **1948**, *40*, 345−348.
(45) Easteal, A. J.; Woolf, L. A. *J. Chem. Thermodyn.* **1985**, *17*, 49−62.
(46) Butler, J. A. V.; Thomson, D. W.; Maclennan, W. H. *J. Chem. Soc.* **1933**, 674−686.
(47) Benson, G. C.; Kiyohara, O. *J. Solution Chem.* **1980**, *9*, 791−804.
(48) Safarov, J.; Heydarov, S.; Shahverdiyev, A.; Hassel, E. *J. Chem. Thermodyn.* **2004**, *36*, 541−547.
(49) Berendsen, H. J. C.; Postma, J. P. M.; van Gunsteren, W. F.; DiNola, A.; Haak, J. R. *J. Chem. Phys.* **1984**, *81*, 3684−3690.
(50) Ryckaert, J. P.; Ciccotti, G.; Berendsen, H. J. C. *J. Comput. Phys.* **1977**, *23*, 327−341.
(51) Darden, T.; York, D.; Pedersen, L. *J. Chem. Phys.* **1993**, *98*, 10089−10092.
(52) Chitra, R.; Smith, P. E. *J. Phys. Chem. B* **2000**, *104*, 5854−5864.
(53) Smith, P. E.; van Gunsteren, W. F. *J. Chem. Phys.* **1994**, *100*, 3169−3174.
(54) Smith, P. E.; van Gunsteren, W. F. *Chem. Phys. Lett.* **1993**, *215*, 315−318.
(55) Daura, X.; Mark, A. E.; van Gunsteren, W. F. *J. Comput. Chem.* **1998**, *19*, 535−547.
(56) *Handbook of Chemistry and Physics*, 66 ed.; CRC Press: Boca Raton, FL, 1985;
(57) McClellan, A. L. *Tables of Experimental Dipole Moments*; Rahara Enterprises: El Cerrito, CA, 1989.
(58) Dixit, S.; Crain, J.; Poon, W. C. K.; Finney, J. L.; Soper, A. K. *Nature* **2002**, *416*, 829−832.
(59) Yamaguchi, T.; Hidaka, K.; Soper, A. K. *Mol. Phys.* **1999**, *96*, 1159−1168.
(60) Yamaguchi, T.; Hidaka, K.; Soper, A. K. *Mol. Phys.* **1999**, *97*, 603−605.
(61) Dixit, S.; Poon, W. C. K.; Crain, J. *J. Phys.*: *Condens. Matter* **2000**, *12*, L323-L328.
(62) Neumann, M. *Mol. Phys.* **1986**, *57*, 97−121.
(63) Neumann, M. *J. Chem. Phys.* **1985**, *82*, 5663−5672.
(64) Oster, G.; Kirkwood, J. G. *J. Chem. Phys.* **1943**, *11*, 175−178.
(65) Denbigh, K. G. *Trans. Faraday Soc.* **1940**, *36*, 936−948.
(66) Berens, P. H.; Mackay, D. H. J.; White, G. M.; Wilson, K. R. *J. Chem. Phys.* **1983**, *79*, 2375−2389.
(67) Wadso, I. *Acta Chem. Scand.* **1966**, *20*, 544−552.
(68) Hruby, J.; Klomfar, J.; Sifner, O. *J. Chem. Thermodyn.* **1993**, *25*, 1229−1242.
(69) Hurle, R. L.; Woolf, L. A. *Aust. J. Chem.* **1980**, *33*, 1947−1952.
(70) Smith, R. L.; Lee, S. B.; Komori, H.; Arai, K. *Fluid Phase Equilib.* **1998**, *144*, 315−322.
(71) Mikhail, S. Z.; Kimel, W. R. *J. Chem. Eng. Data* **1961**, *6*, 533−537.
(72) Benjamin, L.; Benson, G. C. *J. Am Chem. Soc* **1963**, *67*, 858−861.
(73) Derlacki, Z. J.; Easteal, A. J.; Edge, A. V. J.; Woolf, L. A.; Roksandic, Z. *J. Phys. Chem.* **1985**, *89*, 5318−5322.